



Formation Mechanisms of Iron Oxide and Iron Sulfide at High Temperature in Aqueous H₂S Corrosion Environment

Shujun Gao,^{1b} Bruce Brown, David Young, Srdjan Nesic, and Marc Singer

Institute for Corrosion and Multiphase Flow Technology, Department of Chemical & Biomolecular Engineering, Ohio University, Athens, Ohio 45701, USA

Previous high temperature studies have shown that, in an oxygen-free aqueous H₂S environment, magnetite (Fe₃O₄) forms as an inner layer while iron sulfides are found in the outer layer. Although magnetite is thermodynamically less stable than iron sulfide, it was always observed as a defined inner layer. In this work, experiments were conducted to investigate the formation mechanisms of magnetite and iron sulfide in an H₂S environment at high temperature. The corrosion behavior of mild steel was first investigated in environments with and without H₂S at pH 4.0 and 120°C, showing that magnetite is the dominant corrosion product layer in the initial stage of corrosion, due to a much higher saturation value than iron sulfide (mackinawite). In another experiment, the conversion of magnetite into mackinawite was investigated by exposing a preformed magnetite layer on an inert metal (nickel) to an H₂S environment. Consequently, it is postulated that Fe₃O₄ experiences a simultaneous and continuous process of formation at the steel/magnetite interface and conversion to mackinawite at the magnetite/mackinawite interface. A descriptive model for the formation mechanisms of magnetite and iron sulfide at high temperature is presented.

© 2018 The Electrochemical Society. [DOI: 10.1149/2.0921803jes]

Manuscript submitted December 4, 2017; revised manuscript received February 26, 2018. Published March 6, 2018.

Persistent energy demand moves the exploration and production of hydrocarbons towards ever deeper and harsher reservoirs, both onshore and offshore. These wells are frequently operated under high temperature and high pressure conditions in the presence of H₂S.¹⁻⁴ As a result, these operating environments present a constant challenge for new developments in materials selection, design technology, corrosion management, and corrosion modeling in the oil and gas industry.⁵⁻⁸

H₂S corrosion at low temperature (<80°C) has been extensively investigated in the past decades; some of the key issues have been well understood.⁹⁻¹³ However, at elevated temperatures (>80°C), the mechanisms of H₂S corrosion have not been sufficiently studied and many aspects of corrosion kinetics and layer formation processes remain unclear.

The authors' previous research conducted at four elevated temperatures levels, 80°C, 120°C, 160°C, and 200°C, has shown that the initial corrosion rate increases with increasing temperature while the final stable corrosion rate decreased with temperature.^{14,15} Mackinawite, troilite, pyrrhotite, and pyrite were identified as the main iron sulfide phases in the outer layer at 80°C, 120°C, 160°C, and 200°C, respectively. Iron oxide was also detected as an inner layer at every studied temperature and was later identified as magnetite (Fe₃O₄) by electron diffraction performed in a transmission electron microscope (TEM).¹⁶ Thermodynamically, Fe₃O₄ is less stable than any iron sulfide and should not be present in an H₂S dominated environment.¹³ Indeed, it was never reported in similar environments at low temperature.¹⁷ However, further experiments with different test durations, ranging from 1 to 21 days, showed that Fe₃O₄ does not disappear as expected based on thermodynamic arguments, and was persistently found as an inner layer with a relatively constant thickness of 25 μm,¹⁷ as shown in Figure 1.

Reviewing these results, two interesting gaps in understanding can be identified:

1. The corrosion rate quickly decreased in the first day from 5.5 to 2 mm/yr (see dark blue data points in Figure 1). Yet, it is not entirely clear which layer, Fe₃O₄ or mackinawite, was responsible for the decrease of the corrosion rate. Was there a sequence in the layer formation? How fast are these layers forming?
2. The thickness of inner Fe₃O₄ layer did not change significantly with time (20 to 30 μm from day 1 to day 21), while the outer iron sulfide layer kept growing with time from 5 μm to 90 μm after 21 days (see light blue and red data points in Figure 1). So what was the layer growth mechanism of iron sulfide in the presence of an inner Fe₃O₄ layer?

Hypotheses

The following hypotheses were proposed to address the above two questions:

1st Hypothesis: At high temperature, due to a high saturation value, Fe₃O₄ rapidly forms during the initial stage (first day) of corrosion. The growth rate of the Fe₃O₄ layer gradually decreases as the corrosion rate, and consequently the rate of Fe²⁺ ion release, decreases. At the same time, the conversion of Fe₃O₄ to FeS proceeds. The process eventually reaches a steady state when the rate of Fe₃O₄ formation and conversion become equal, leading to a constant Fe₃O₄ layer thickness.

2nd Hypothesis: At high temperature, iron sulfide growth mechanism is mainly through a conversion from Fe₃O₄. The Fe₃O₄ simultaneously forms at the steel/Fe₃O₄ interface and converts to FeS at the Fe₃O₄/FeS interface.

Methodology

To test the 1st hypothesis, Experimental Set #1 was conducted, as shown in Figure 2:

- Step 1: A X65 carbon steel specimen was immersed into 1 wt% NaCl solution (purged by N₂) without H₂S. The experimental condition was 120°C at an initial pH 4.0. After 1 day, the specimen with preformed Fe₃O₄ layer was retrieved, immediately rinsed with deionized water and isopropanol, dried by N₂ flow, and stored in a nitrogen atmosphere. This step took less than 10 min.

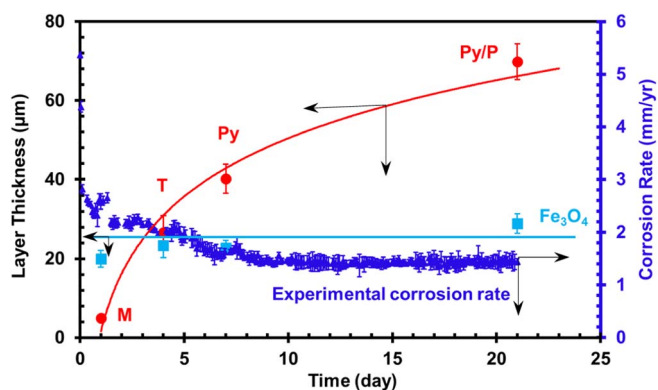


Figure 1. Corrosion rate and layer thickness of Fe₃O₄ and iron sulfide change with time, 1 wt% NaCl solution, T = 120°C, pH₂S = 0.1 bar, pH = 4.0 (initial) ~ 5.5 (final), M: mackinawite, T: troilite, Py: pyrrhotite, P: pyrite.

²E-mail: sg389813@ohio.edu

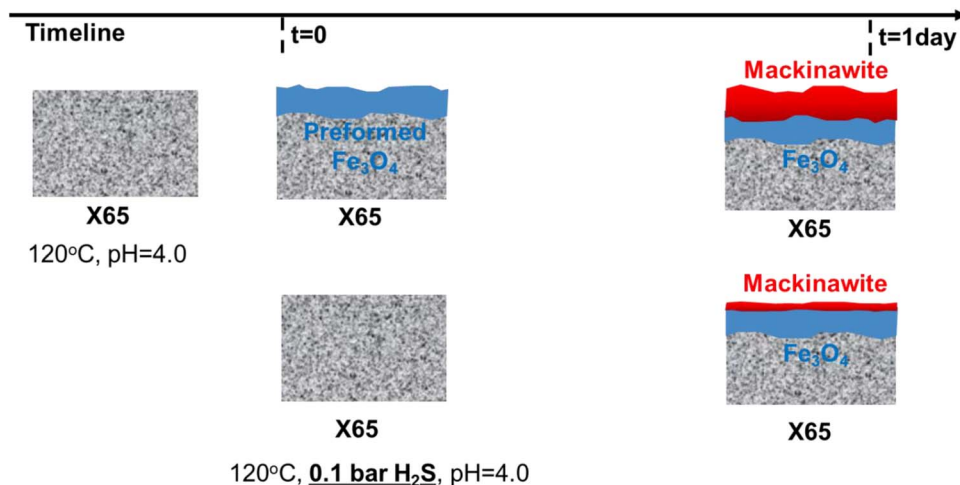


Figure 2. Experiment design to test hypothesis #1.

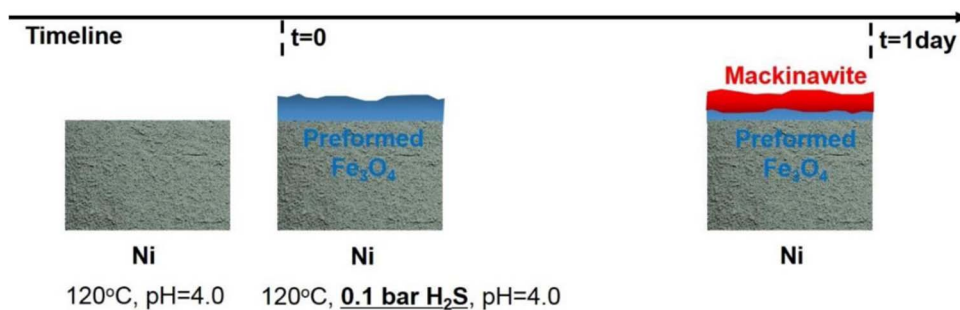


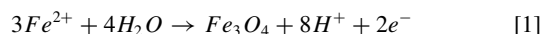
Figure 3. Experiment design to test hypothesis #2.

- Step 2: The preformed Fe_3O_4 carbon steel specimen was exposed under the same condition (1 wt% NaCl solution, 120°C , initial pH 4.0) containing 0.1 bar H_2S , for 1 day. The transfer step took around 15 min.

According to the 1st hypothesis, the iron sulfide layer growth should be dominant in Step 2, since the initial Fe_3O_4 layer formation step would have already been completed. Therefore, a much thicker iron sulfide (mackinawite) layer would form compared with the same experiment conducted with no preformed Fe_3O_4 layer (see Figure 2 and the first point in Figure 1).

To verify the 2nd hypothesis, the Experimental Set #2 was performed, as shown in Figure 3:

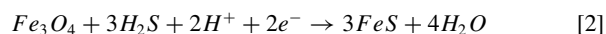
- Step 1: Nickel (Ni) specimens, which should not corrode in the current experimental conditions with or without H_2S , were immersed into a 1 wt% NaCl solution (purged by N_2) without H_2S . Some X65 steel specimens were also immersed in the cell at the same time solely to act as a source of Fe^{2+} . The test condition was still 120°C at an initial pH 4.0. This was done in order to precipitate Fe_3O_4 on the Ni surface via Reaction 1:



The cathodic reaction(s) associated with Reaction 1 is not identified with certainty as of yet but it is postulated that H^+ reduction and H_2S reduction could be involved.

- Step 2: The Ni specimens with preformed Fe_3O_4 were exposed to a 0.1 bar H_2S environment under the same conditions (120°C , initial pH 4.0) for 1 day. The estimated time for the whole procedure is the same as the above Experimental Set #1.

Based on the 2nd hypothesis, the preformed Fe_3O_4 layer should convert to iron sulfide in Step 2, via Reaction 2. Since there was no replenishment for Fe from the steel substrate to form new Fe_3O_4 (Reaction 1), the Fe_3O_4 found at the end of Step 2 should be either very thin or even non-existent if it completely converted to iron sulfide.



The anodic reaction(s) associated with Reaction 2 is also not clearly identified but it could be a combination of Ni, H_2S , H_2O or H_2 oxidations – Ni and H_2S oxidations being more likely.

H_2S corrosion experiments were conducted in a 7 L Hastelloy autoclave, shown in Figure 4. Linear polarization resistance (LPR) measurements were carried out in a conventional three-electrode electrochemical setup using a potentiostat. The working electrode was a

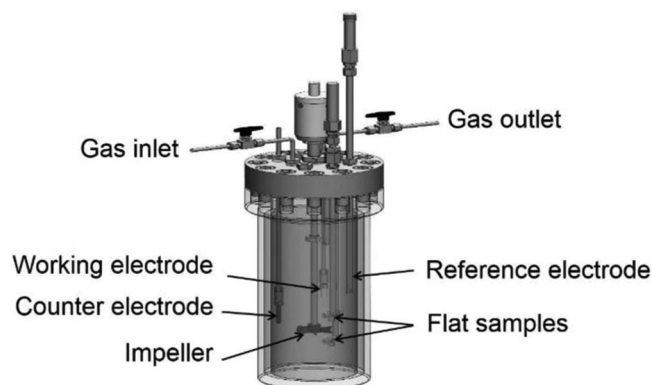


Figure 4. Experimental autoclave setup.

Table I. Chemical composition of API 5L X65 carbon steel (wt%).

Cr	Mo	S	V	Si	C	P	Ni	Mn	Fe
0.14	0.16	0.009	0.047	0.26	0.13	0.009	0.36	1.16	Balance

cylindrical UNS K03014 (API 5L X65) carbon steel, its chemical composition is shown in Table I. A Pt-coated Nb cylinder served as the counter electrode. Due to the lack of a reliable reference electrode in the high temperature H₂S environment, a commercial Zr/ZrO₂ high-temperature, high-pressure electrode with a pH probe was used as a pseudo-reference electrode. This is doable as long as its potential is stable under the experimental conditions, while the exact potential with respect to an SHE is unknown.¹⁸ Some flat specimens were fastened to a fixed shaft using a PTFE-coated 304SS wire. A centrally positioned impeller with 1000 rpm rotation speed was used to keep the solution well mixed during each experiment.

The experimental conditions such as pH and partial pressure of H₂S (pH₂S), summarized in Table II, were calculated based on an in-house water chemistry model (reviewed in previous publications).¹⁴ Before each experiment, the carbon steel and nickel specimens were polished with 400# and 600# grit abrasive paper, then thoroughly rinsed with deionized water and isopropanol. The 1 wt% NaCl solution in the autoclave was purged with N₂ overnight at room temperature. Then the pH was adjusted by deoxygenated 0.1 M HCl solution according to the water chemistry calculation and H₂S was added to the autoclave at room temperature to achieve a solution pH of 4.0 and desired 0.1 bar pH₂S when the temperature reached 120°C. N₂ (research grade 99.9997%) and H₂S (99.5% minimum) were purchased from Air Gas. 10% H₂S and 90% N₂ were premixed into a gas cylinder and were used to achieve 0.10 bar H₂S in the autoclave. Then the lid with the mounted specimens was mounted on the top the autoclave. It took only about 30 min to heat the autoclave from room temperature to 120°C. However, cooling down to around 70°C was much longer (~4 hours) and, for safety concerns, the remaining H₂S was then vented by purging with N₂ for at least 2 hours. After each experiment, the H₂S composition in the gas phase was measured by gas chromatography (GC). It was found that H₂S consumption due to corrosion was negligible.¹⁴ The corroded specimens were retrieved and examined by X-ray diffraction (XRD), scanning electron microscopy/energy dispersive X-ray spectroscopy (SEM/EDS). Full experimental details can be found elsewhere.¹⁴ For the tests without H₂S, the same procedure was followed except that no H₂S was involved.

Results and Discussion

Sequence of Fe₃O₄/FeS formation.—The corrosion rates obtained in Experimental Set #1 with H₂S (0.1 bar), and without H₂S, are shown in Figure 5. The time zero is when the temperature reached 120°C. For clarity, these two are respectively labeled as experiment “with H₂S”, “without H₂S” and “with preformed Fe₃O₄”.

Looking first at the results from experiment “with H₂S” and experiment “without H₂S”, the LPR corrosion rates are both shown to decrease relatively quickly at high temperature. The LPR corrosion rate from experiment “without H₂S” gradually decreased during the first 50 hours of exposure and reached a stable corrosion rate of 0.5 mm/yr. The LPR corrosion rate from experiment “with H₂S” reduced dramatically in the first 2 hours from over 5 mm/yr to about

Table II. Test matrix.

Parameter	Value
Temperature	120°C
pH ₂ S	0.1 bar
Initial pH	4.0
Rotation speed	1000 rpm

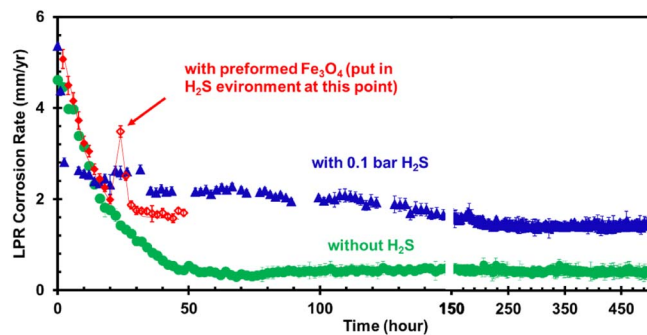


Figure 5. LPR corrosion rate in experiments without H₂S (green), with 0.1 bar H₂S (blue), and with preformed Fe₃O₄ layer for one-day, X65, 1 wt% NaCl solution, T = 120°C, initial pH = 4.0, B = 23 mV/decade, the results are from Experimental Set #1.

2.8 mm/yr. Then it kept decreasing in a slower manner and eventually stabilized around 2 mm/yr.

The results from experiment “with preformed Fe₃O₄” are plotted in red in Figure 5, including the 1 day, representing the time needed to preform the Fe₃O₄ layer. The corrosion rates experienced by the specimen during the Fe₃O₄ layer formation (red dots in Figure 5) were similar to the corrosion rates during the first day of the experiment “without H₂S” (green dots in Figure 5) as would be expected. After the specimen with the preformed Fe₃O₄ was transferred to the H₂S environment at the 1-day mark, the LPR corrosion rate in the experiment “with preformed Fe₃O₄” started at 3.5 mm/yr, which is lower than the initial LPR rate obtained the experiment “with H₂S” (5.5 mm/yr). This result demonstrates that the Fe₃O₄ layer alone offers additional protection in an H₂S environment. The relatively high initial corrosion rate (3.5 mm/yr) value could be due to some cracking and/or spalling, created when the specimen was transferred, as the Fe₃O₄ layer was expected to provide higher initial corrosion protection in the H₂S environment. The corrosion rate did decrease sharply in the next few hours of exposure but stabilized at 1.8 mm/yr, similarly to the final rate in the experiment “with H₂S”. In comparison, a higher protectiveness by the Fe₃O₄ layer was clearly demonstrated in an environment without H₂S at the same high temperature.¹⁹

It has been demonstrated that a thin mackinawite layer can immediately form and slow down the corrosion rate when the steel is exposed to aqueous H₂S.¹² The same phenomenon appears in our study: with H₂S, the corrosion rate quickly dropped in the first 5 hours. Without H₂S, the drop of the corrosion rate is not as abrupt as with H₂S, it gradually decreased up to 40 hours, but ended up with a much lower corrosion rate. This suggests that the overall protectiveness of Fe₃O₄ is better than mackinawite. Obviously, both Fe₃O₄ and mackinawite are responsible for the decrease of corrosion rate. Fe₃O₄ and mackinawite have different electronic properties. For example, Fe₃O₄ has been reported to be a very good electrical conductor,²⁰ while iron sulfides are considered as semi-conductor.²¹ Consequently, different layers should have different roles on corrosion.^{14,22}

The experiments were performed in the same environment (0.1 bar H₂S or N₂) considering different exposure times (1, 4, 7, and 21 days). Each of these exposure time represents one single test. Consequently, the tests were repeated - just not for the same duration. The repeatability of the tests performed in N₂ environment is shown in Figure 6. Here the repeatability is very good over all the exposure time tested. The repeatability of H₂S experiments is addressed in prior publications.^{14–16} Experimental results never overlap perfectly due to the inherent difficulty of conducting autoclave experiments in H₂S environments. Although good repeatability is difficult to obtain, it should be stressed that the conditions at the start and end of the tests are clearly documented. This is a great improvement compared to any prior similar studies which never actually acknowledge changing experimental conditions during the tests (mostly in water chemistry).^{23–25}

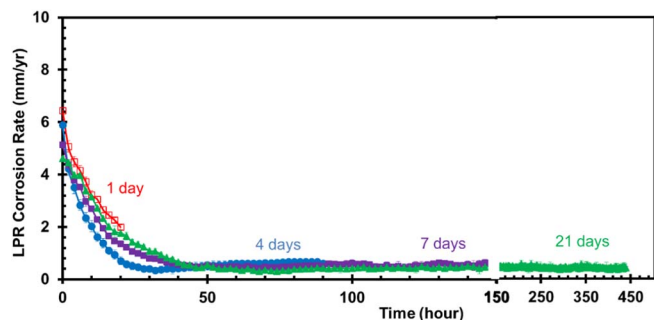


Figure 6. LPR corrosion rate in N_2 -only experiments with different exposure time, showing good repeatability. X65, 1 wt% NaCl solution, $T = 120^\circ\text{C}$, initial pH = 4.0, $B = 23$ mV/decade.

It is also important to point out that some corrosion products could already form during the heating up period. For the experiments without H_2S , the only possible corrosion product that can form is still Fe_3O_4 .¹³ This would not affect the results. For the experiments with H_2S , a thin iron sulfide film could form within seconds.¹² Unfortunately, this is not avoidable in the experiments, even for low temperature experiments in a glass cell.

The corrosion products from the experiment “without H_2S ” at high temperature were characterized by XRD after different test durations, as shown in Figure 7. All the corrosion products were identified as pure (entirely) magnetite (Fe_3O_4) regardless of the exposure time. The intensity of the peaks also did not increase with time and the α -Fe matrix was already undetectable after the 1 day experiment. This means that the Fe_3O_4 became very thick and compact rapidly, implying good corrosion protection properties. The EDS mapping scan, Figure 8, also confirms that the layer was comprised of iron (Fe) and oxygen (O). The thickness after 1 day of exposure was approximately $25\ \mu\text{m}$, which is appropriately the same value as the thickness of the oxide layer obtained from experiment “with H_2S ” for 1 day, as shown in Figure 1 and Figure 8. The fact that the two Fe_3O_4 layer thicknesses are the same seems to indicate that the Fe_3O_4 growth during the first

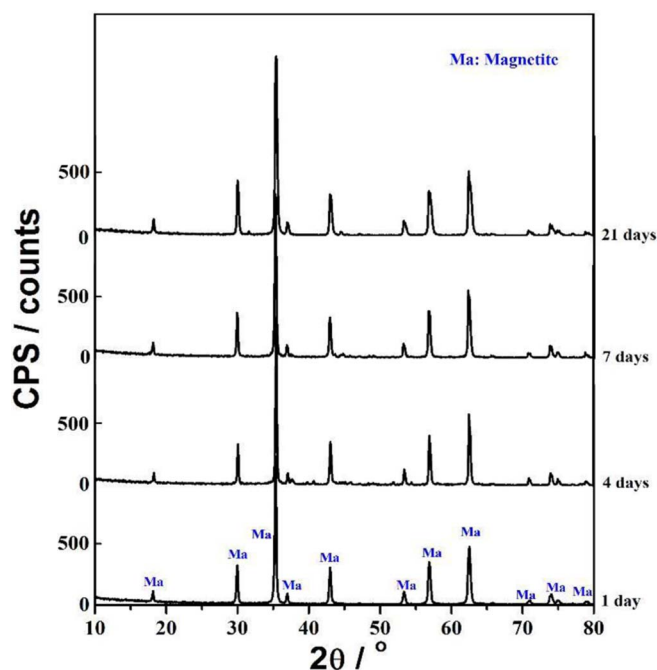


Figure 7. XRD patterns of X65 specimen in experiment without H_2S after different test durations, 1 wt% NaCl solution, N_2 purged, $T = 120^\circ\text{C}$, initial pH = 4.0.

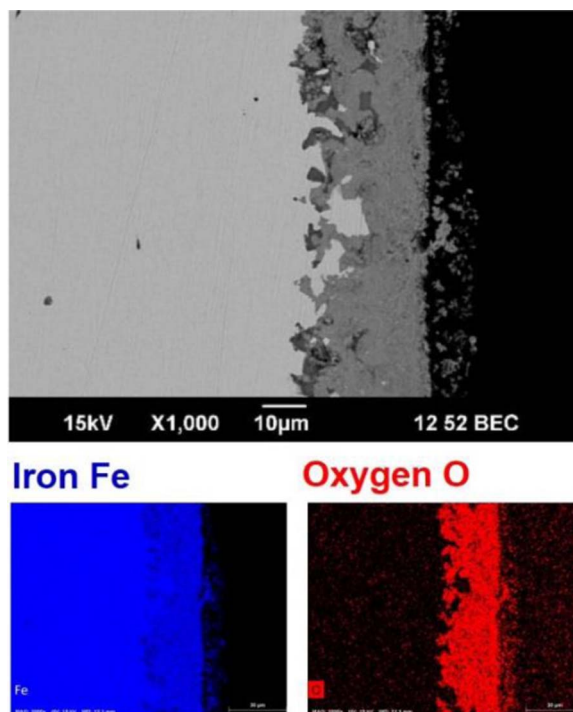


Figure 8. Cross-section and EDS mapping results for X65 specimen in experiment without H_2S after 1 day, 1 wt% NaCl solution, $T = 120^\circ\text{C}$, initial pH = 4.0.

day of testing occurs with little interference from H_2S . Consequently, it is proposed that the Fe_3O_4 formation was dominant in the first few hours of testing at high temperature even with H_2S . This is discussed in more details below.

The cross-sections of specimens from the experiment “without H_2S ” are shown in Figure 9. It can be seen that the overall layer thickness increased from $25\ \mu\text{m}$ after 1 day to $80\ \mu\text{m}$ after 21 days. Comparing the growth behavior of Fe_3O_4 (without H_2S , Figure 10) and iron sulfide (with H_2S , Figure 1), the same trend is observed. This could be a coincidence, especially since the thickness of the Fe_3O_4 layer alone stayed at $\sim 25\ \mu\text{m}$ in the experiment “with H_2S ” and did not

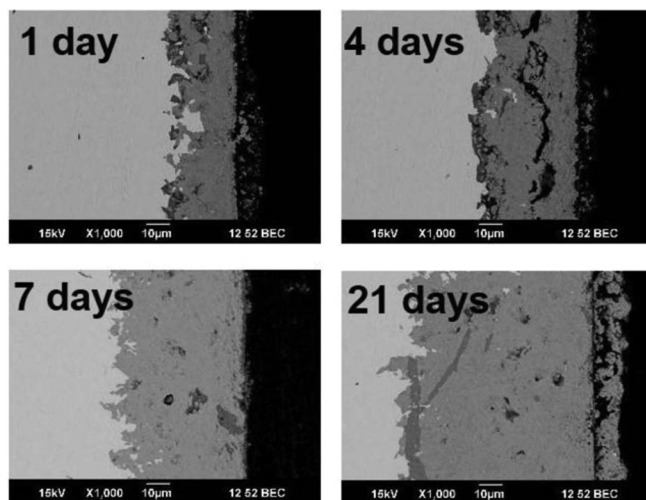


Figure 9. The growth of Fe_3O_4 layer with time, shown by cross-sections of X65 specimen in the experiment without H_2S after different test durations (obtained in separate experiments), 1 wt% NaCl solution, $T = 120^\circ\text{C}$, initial pH = 4.0.

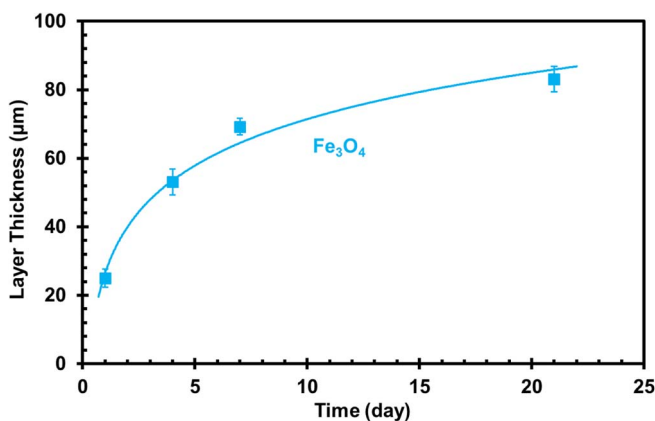


Figure 10. The thickness of Fe_3O_4 layer with time in the experiment without H_2S , X65, 1 wt% NaCl solution, $T = 120^\circ\text{C}$, initial $\text{pH} = 4.0$.

increase further with exposure time. However, this could also indicate that the FeS and the Fe_3O_4 formation rates are inherently linked. This, again, highlights the complexity of the growth mechanism of iron sulfide in the presence of a Fe_3O_4 layer, which will be discussed later.

The X65 steel specimen with preformed Fe_3O_4 was exposed to a 0.1 bar H_2S environment under the same conditions (Table II) for another day. The experiments “with H_2S ” and “without H_2S ” also lasted 1 day. The EDS mapping results for the cross-sections are shown in Figure 11; all images are at the same magnification for ease of comparison. However, the data related to the experiment “with H_2S ” were obtained using a different EDS detector than for the other two conditions and the display of the results can be more difficult to interpret. In the first row of Figure 11, the highest magnitude concentration of elements is indicated by white pixels and lowest magnitude by blue pixels; in the other two rows, the brightness intensity of the same-color pixels is related to the concentration. The level of color brightness can only be used in a qualitative way and can be compared from image to image. In terms of Fe_3O_4 layer thickness for the specimen with, without H_2S , and with preformed Fe_3O_4 layer, no significant difference can be found. However, the thickness of the outer iron sulfide

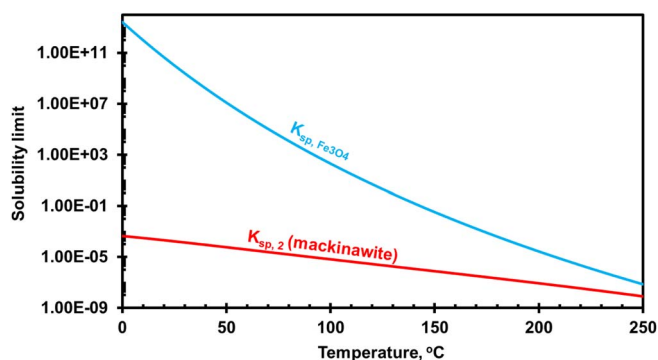
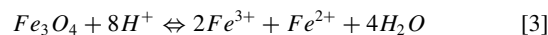


Figure 12. Solubility limit for Fe_3O_4 and mackinawite with the increase of temperature, $\text{pH} = 4.0$, $\text{pH}_2\text{S} = 0.1$ bar.

layer, represented by sulfur (S) content, greatly increased from less than $5 \mu\text{m}$ without the preformed Fe_3O_4 layer to $30 \mu\text{m}$ with the preformed Fe_3O_4 layer.

These experimental results infer that the formation rate of Fe_3O_4 is faster than that of iron sulfide at the tested temperature. This explains why Fe_3O_4 is persistently detected while not being thermodynamically favored. In comparison, the presence of Fe_3O_4 was not reported at lower temperature in similar environments. A deeper look into the solubility limit of each corrosion product can help explain this behavior.

The solubility equilibria for Fe_3O_4 and mackinawite are given by Reactions 3 and 6 with the corresponding solubility limit expressions given by Equations 4 and 7. The Gibbs energy change ΔG for Reaction 3 is given in Equation 5. The effect of temperature on the solubility limit is shown in Figure 12. The solubility limit for Fe_3O_4 experiences a significant drop with the increase of temperature, while in comparison, for mackinawite, the decrease in solubility limit is only moderate.^{26,27}



$$K_{sp, \text{Fe}_3\text{O}_4} = e^{-\frac{\Delta G}{RT}} \quad [4]$$

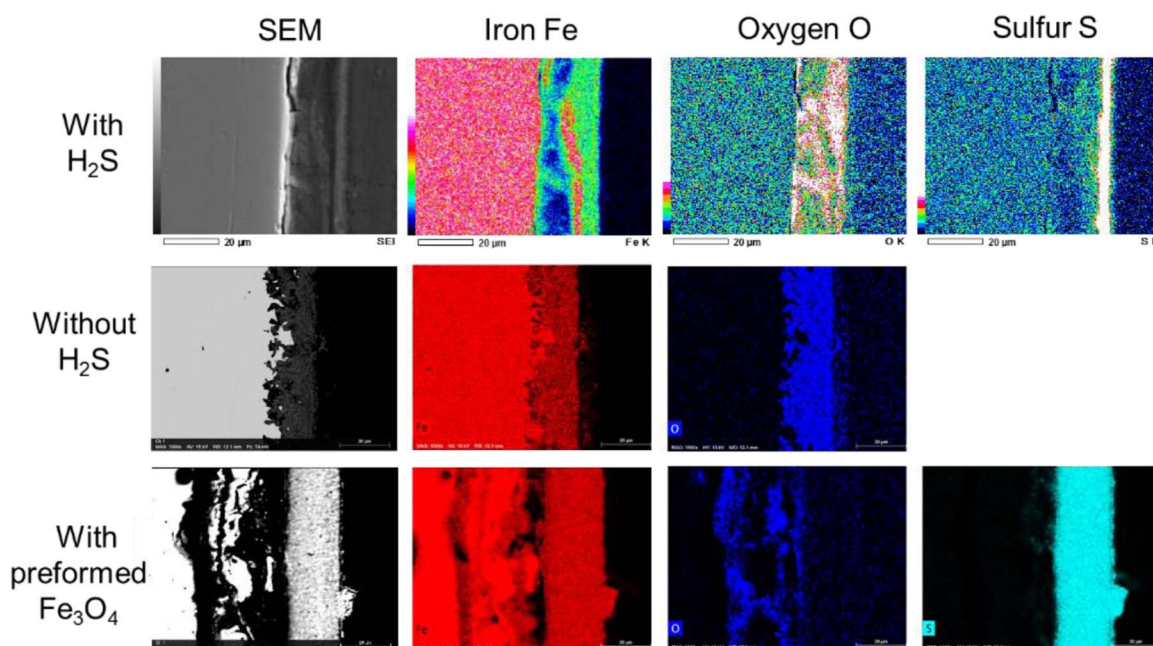


Figure 11. EDS mapping results for X65 specimen from the experiment without H_2S with, with 0.1 bar H_2S , and with preformed Fe_3O_4 layer, 1 wt% NaCl solution, $T = 120^\circ\text{C}$, initial $\text{pH} = 4.0$.

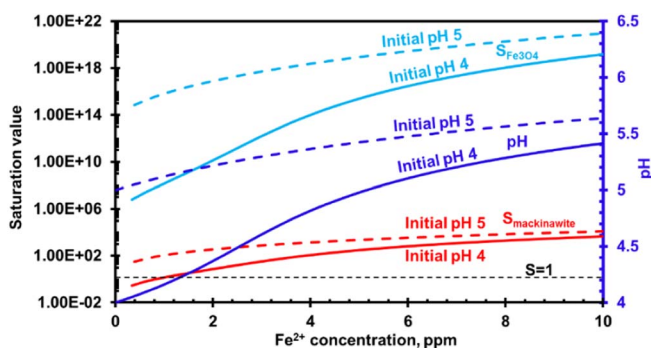


Figure 13. Saturation value for Fe_3O_4 and mackinawite at initial pH 4.0 and 5.0, $[\text{Fe}^{3+}] = 1 \times 10^{-10} \text{ M}$, $T = 120^\circ\text{C}$, $p\text{H}_2\text{S} = 0.1 \text{ bar}$.

$$\Delta G = 2\Delta G(\text{Fe}^{3+}) + \Delta G(\text{Fe}^{2+}) + 4\Delta G(\text{H}_2\text{O}) - \Delta G(\text{Fe}_3\text{O}_4) - 8\Delta G(\text{H}^+) \quad [5]$$



$$K_{sp,2} = 10^{\frac{2848.779}{T_K} - 6.347 + \log(K_{a,1})} \quad [7]$$

$$K_{a,1} = 10^{782.43945 + 0.361261T_K - 1.6722 \times 10^{-4}T_K^2 - 20565.7315/T_K - 142.7417222 \ln T_K} \quad [8]$$

The level of saturation value governs the precipitation rate and consequently the layer formation/dissolution rate. The expressions for saturation value of Fe_3O_4 ($S_{\text{Fe}_3\text{O}_4}$) and mackinawite ($S_{\text{mackinawite}}$) are given in Equations 9 and 10. Assuming Reaction 3 and 6 are both in equilibrium at 120°C and pH 4.0, i. e., $S_{\text{Fe}_3\text{O}_4} = S_{\text{mackinawite}} = 1$, this gives the ferric ion concentration $[\text{Fe}^{3+}]$ close to $1.0 \times 10^{-10} \text{ M}$, which means the calculated $S_{\text{Fe}_3\text{O}_4}$ may be underestimated compared to earlier similar studies.¹³

$$S_{\text{Fe}_3\text{O}_4} = \frac{[\text{Fe}^{3+}]^2[\text{Fe}^{2+}]}{[\text{H}^+]^8} \quad [9]$$

$$S_{\text{mackinawite}} = \frac{[\text{Fe}^{2+}][\text{HS}^-]}{[\text{H}^+]} \quad [10]$$

As soon as the steel specimen is inserted into an aqueous H_2S environment, iron starts to dissolve and release Fe^{2+} , resulting in an increase in pH (considering a closed system such as an autoclave). Figure 13 shows the changes in $S_{\text{Fe}_3\text{O}_4}$, bulk solution pH, and $S_{\text{mackinawite}}$ with an increase in $[\text{Fe}^{2+}]$ from 0 to 10 ppm in a closed system. The saturation values are based on calculations which only show a trend without consideration of precipitation. By the time the test is started, FeS precipitation could have already been occurring acting as a sink of Fe^{2+} ions and slowing down the rate of increase in saturation. In H_2S environments, the Fe^{2+} concentration is typically between 0 to 5 ppm since the $S_{\text{mackinawite}}$ never reaches very high values due to the fast kinetics of FeS precipitation.^{13,14} At 120°C with an initial pH 4.0, Fe_3O_4 is strongly supersaturated ($S_{\text{Fe}_3\text{O}_4} = 10^6$) almost immediately after Fe^{2+} ions are generated in the solution. In contrast, $S_{\text{mackinawite}}$ requires at least 0.8 ppm of Fe^{2+} to reach a saturation of 1. Obviously, Fe_3O_4 is expected to precipitate faster and dominate the layer growth during the initial stage, because $S_{\text{Fe}_3\text{O}_4}$ is at least six orders of magnitude greater than $S_{\text{mackinawite}}$ and highly supersaturated. However, the solution pH will increase with time and this could change the ratio of saturation levels. Figure 13 also presents the saturation values at initial pH 5.0. However, the difference between initial $S_{\text{Fe}_3\text{O}_4}$ and $S_{\text{mackinawite}}$ is even higher at pH 5.0, so mildly acidic environments (pH 4 and pH 5) are not expected to largely affect the sequence and rate of layer growth at the tested temperature.

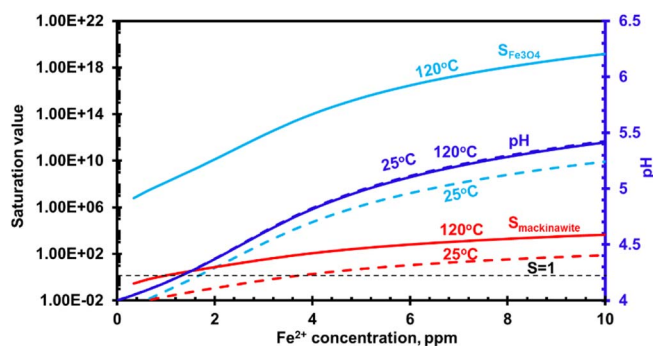


Figure 14. Saturation value for Fe_3O_4 and mackinawite at 25°C and 120°C , $[\text{Fe}^{3+}] = 1 \times 10^{-10} \text{ M}$, $p\text{H}_2\text{S} = 0.1 \text{ bar}$, initial pH = 4.0 (pH lines for 25°C and 120°C overlap in the graph).

Figure 14 presents the trend of $S_{\text{Fe}_3\text{O}_4}$ and $S_{\text{mackinawite}}$ at 25°C and 120°C . It is important to notice that at 25°C and for very low ferrous ion concentrations, $S_{\text{Fe}_3\text{O}_4}$ is of the same magnitude as $S_{\text{mackinawite}}$. The saturation level is indeed related to the kinetics of layer formation but other parameters also affect the reaction rates (activation energy, kinetic rate constant). At low temperature, FeS formation is kinetically favored. Considering that Fe_3O_4 is more soluble at lower temperatures (see Figure 12), this explains why Fe_3O_4 is not found at temperatures below 80°C while it forms very quickly and actually dominates during the initial stages of corrosion at temperatures above 80°C in an H_2S corrosion environment. Temperature is the key influential factor.

In summary, due to a much higher saturation value, Fe_3O_4 is likely to form very quickly, faster than mackinawite, during the initial stages of corrosion at temperatures above 80°C in aqueous H_2S corrosion environments. A thin mackinawite layer is expected to immediately form as well when the steel is exposed to $[\text{H}_2\text{S}]_{\text{aq}}$, but the thickness of this layer is in the order of nanometers which is much lower than for Fe_3O_4 ($\sim 25 \mu\text{m}$).¹² Therefore, to be more precisely, simultaneous growth of Fe_3O_4 and mackinawite is then expected to occur, but initially the kinetics for Fe_3O_4 precipitation dominates at high temperatures.

Iron sulfide formation mechanism.—After the initial stages of formation, the iron sulfide growth mechanism was investigated in Experimental Set #2 in order to test the 2nd hypothesis. The experimental design is shown in Figure 3. The Fe_3O_4 precipitation was performed on Ni specimens using Fe^{2+} ions generated by an independently corroding X65 steel specimens immersed in the same solution at 120°C , with an initial pH 4.0 and for 21 days. The Fe_3O_4 did indeed precipitate on the Ni surface, as identified by XRD in Figure 15. A precipitated Fe_3O_4 layer ($\sim 10 \mu\text{m}$) can also be observed from the cross-section analysis in Figure 16 and is confirmed by the EDS mapping scan. This Ni specimen with the preformed Fe_3O_4 layer was retrieved, dried, stored, and then exposed for one day in a 0.1 bar H_2S environment under otherwise same conditions (120°C , initial pH 4.0) to verify the 2nd hypothesis.

After 1 day of exposure, the Ni specimen was retrieved and again characterized by XRD and SEM/EDS, as shown in Figure 15 and Figure 16. The Fe_3O_4 layer disappeared and was totally replaced by a mackinawite layer as confirmed by both XRD and EDS. The EDS mapping results show an iron sulfide layer on the Ni surface with no obvious oxygen (O) detected.

The above results seem to validate the 2nd hypothesis, stating that the FeS layer grows through Fe_3O_4 conversion. Without H_2S present, the Fe_3O_4 layer increased in thickness over time (Figure 10). With H_2S present, the Fe_3O_4 layer stabilized at a specific thickness while the iron sulfide layer increased in thickness with time due to the conversion reaction (Figure 1). Coincidentally, the FeS growth rate is similar to the rate of formation of the Fe_3O_4 layer observed in Figure 10; which is a further evidence that Fe_3O_4 kept growing and converting to iron

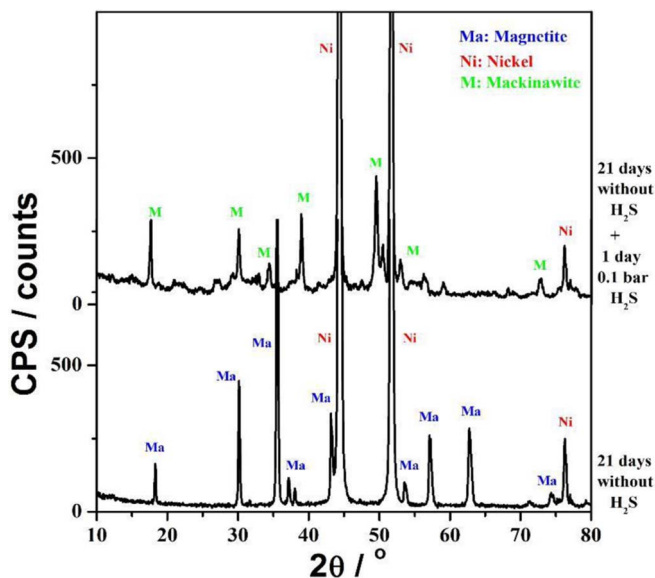


Figure 15. XRD patterns of preformed Fe_3O_4 layer on Ni specimen before and after H_2S was introduced, 1 wt% NaCl solution, $T = 120^\circ\text{C}$, initial $\text{pH} = 4.0$.

sulfide in the aqueous H_2S environment. However, FeS precipitation via Reaction 6 cannot be entirely excluded since $S_{\text{mackinawite}}$ did exceed 1. However, previous results show that the Fe^{2+} concentration was around 5 ppm,¹⁴ which gives a $S_{\text{mackinawite}}$ value around 10 (Figure 13). This value of saturation is not extremely high and would not constitute a high driving force to produce a significant amount of precipitated iron sulfide. A recent corrosion prediction model developed by Zheng, et al.,²⁸ which includes iron sulfide precipitation, predicts the iron sulfide layer thickness to be below $14 \mu\text{m}$ after 7 days. Compared with the result in Figure 1, the thickness of iron sulfide was above $45 \mu\text{m}$ after 7 days. This further demonstrates that the main contribution to iron sulfide growth at higher temperatures was through the Fe_3O_4 conversion mechanism rather than the precipitation mechanism.

Recall the conclusion from hypothesis #1: the Fe_3O_4 formation was dominant at the initial stage of corrosion due to high saturation value. Actually, it is hypothesized that it was dominant over the whole test duration, not only at the start of the test. However, the Fe_3O_4 layer was thermodynamically less stable and kept converting to iron sulfide. The rate of conversion from Fe_3O_4 to FeS eventually matched the rate of Fe_3O_4 formation.

Descriptive model for the $\text{Fe}_3\text{O}_4/\text{FeS}$ formation mechanisms at high temperature.—Based on the experimental results, a descriptive model for Fe_3O_4 and FeS formation mechanisms at high temperature is shown in Figure 17 and presented below:

- X65 carbon steel is exposed to H_2S corrosion environment at high temperature. Fe starts to dissolve and releases Fe^{2+} ions in the solution, as shown in Figure 17a;
- Fe^{2+} reacts with its surrounding H_2O molecules and Fe_3O_4 forms quickly via Reaction 1. Fe_3O_4 layer is protective and the corrosion rate (i.e. the rate of Fe^{2+} ions release) decreases. Consequently, the formation rate of Fe_3O_4 also decreases which slows down the layer growth rate. Simultaneously, as shown in Figure 17b, the aqueous H_2S diffuses from the bulk solution, through the iron sulfide layer, to the $\text{Fe}_3\text{O}_4/\text{FeS}$ interface, through the iron sulfide layer, to the $\text{Fe}_3\text{O}_4/\text{FeS}$ interface, which transforms it to iron sulfide via Reaction 2 but initially at a much lower rate than Fe_3O_4 formation;
- Iron sulfide formation through Fe_3O_4 conversion catches up as the formation of Fe_3O_4 slows down. Fe_3O_4 continuously forms at the metal surface and converts to iron sulfide at the $\text{Fe}_3\text{O}_4/\text{FeS}$ interface, as shown in Figure 17c. Eventually, the whole process reaches a steady state: these two reactions occur at a similar rate which stabilizes the thickness of the Fe_3O_4 layer;
- Some Fe^{2+} diffuses from the steel surface, through Fe_3O_4 layer, and meets HS^- . If the saturation value exceeds the solubility limit of iron sulfide, iron sulfide will precipitate at the FeS/solution interface and the FeS layer will grow even further, as shown in Figure 17d.

Other research studies^{29–31} suggested alternative pathways for the layer growth mechanism, either stating that both Fe_3O_4 and FeS layers grow solely through precipitation (the present work suggests that precipitation is only a minor contributor) or postulating that the layer growth is linked to Fe solid state outward diffusion through the Fe_3O_4 lattice. However, the experimental results presented here do not seem to validate either of these mechanisms.

Conclusions

- Due to the higher kinetics at high temperature, a Fe_3O_4 layer is the dominant corrosion product forming at the steel surface in the initial stages of experiments where steel is exposed to an acidic aqueous H_2S environment.
- Both Fe_3O_4 and mackinawite are responsible for the initial rapid decrease of the corrosion rate observed in sour environment at high temperature, but Fe_3O_4 provides a better protection in the long run.

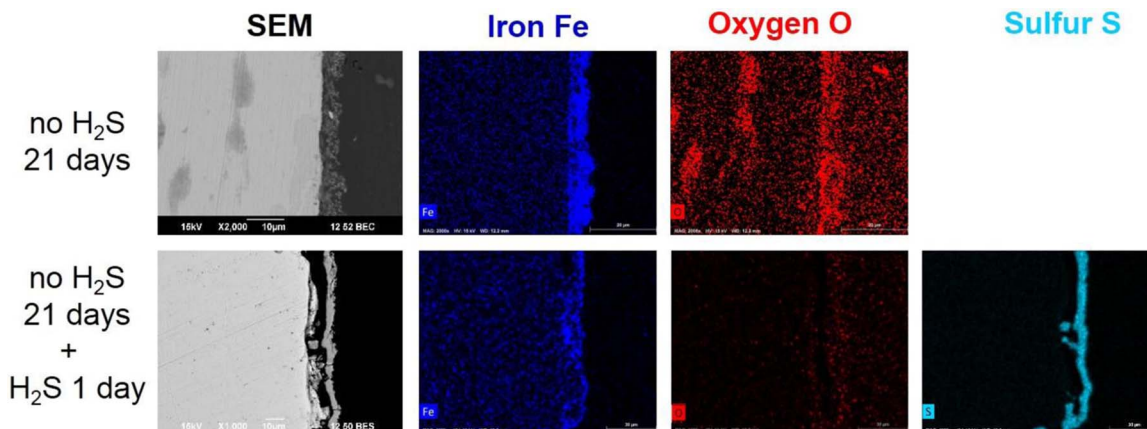


Figure 16. EDS mapping results for the cross section of preformed Fe_3O_4 layer on Ni specimen before and after H_2S was introduced, 1 wt% NaCl solution, $T = 120^\circ\text{C}$, $\text{pH}_2\text{S} = 0.1$ bar, initial $\text{pH} = 4.0$.

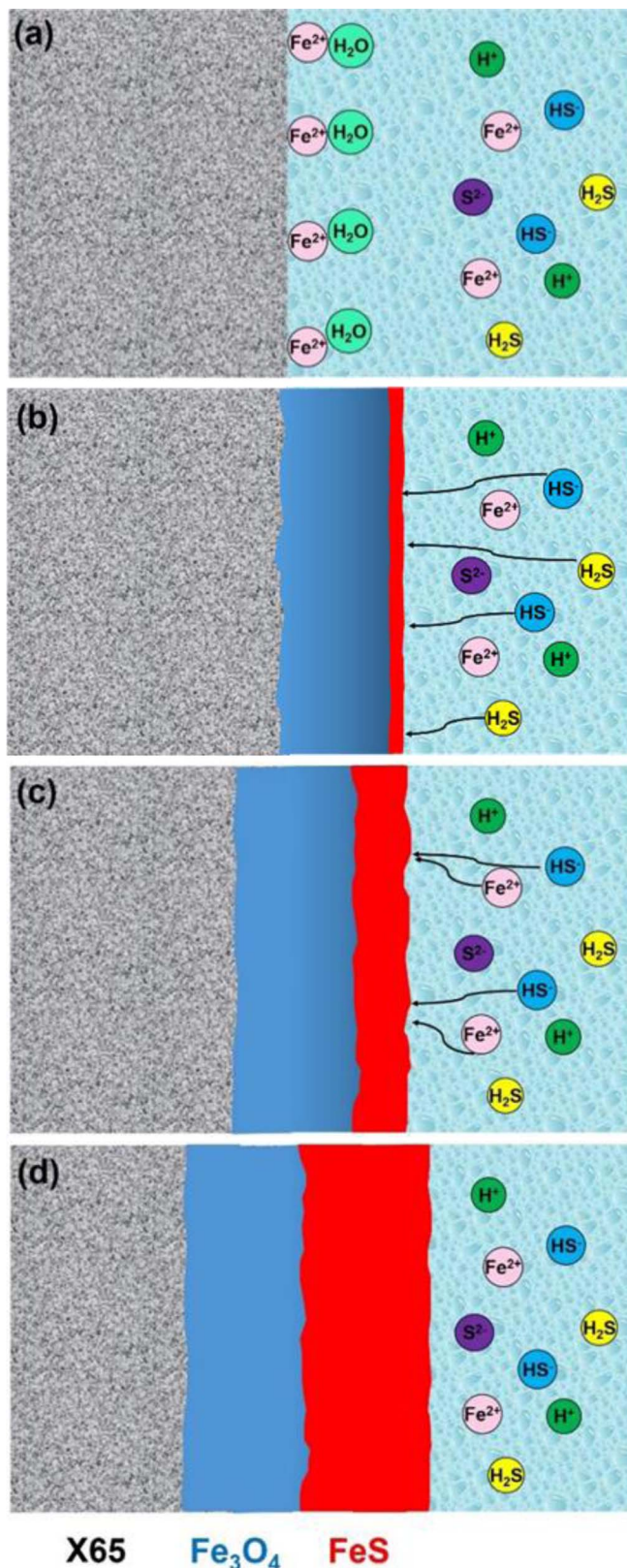


Figure 17. Schematic diagrams for Fe₃O₄/FeS formation mechanisms at higher temperatures in an H₂S environment.

- Fe₃O₄ converts to mackinawite since it is thermodynamically less stable than iron sulfide. Fe₃O₄ experiences a simultaneous and continuous process of formation, at the steel/Fe₃O₄ interface, and transformation to FeS, at the Fe₃O₄/FeS interface.

Acknowledgment

The authors would like to express sincere appreciation to the following industrial sponsors for their financial support and direction: Anadarko, Baker Hughes, BP, Chevron, CNOOC, ConocoPhillips, DNV GL, ExxonMobil, M-I SWACO (Schlumberger), Multi-Chem (Halliburton), Occidental Oil Company, Petrobras, PTT, Saudi Aramco, Shell Global Solutions, SINOPEC (China Petroleum), TransCanada, TOTAL, and Wood Group Kenny.

ORCID

Shujun Gao  <https://orcid.org/0000-0002-3149-9911>

References

1. G. DeBruijn, "High-pressure, high-temperature technologies," *Oilfield Rev.*, **20**, 46 (2008).
2. H. J. Chen, *High temperature corrosion inhibition performance of imidazoline and amide, no. 00035*, NACE International, San Antonio, TX (2010).
3. S. S. Prabha, "Corrosion problems in petroleum industry," *Eur. Chem. Bull.*, **3**, 300 (2014).
4. S. Gao, C. Dong, A. Fu, K. Xiao, and X. Li, "Corrosion behavior of the expandable tubular in formation water," *Int. J. Min. Met. Mater.*, **22**, 149 (2015).
5. S. Ramachandran, C. Menendez, V. Jovancevic, and J. Long, "Film persistency of new high temperature water-based batch corrosion inhibitors for oil and gas wells," *J. Pet. Explor. Prod. Technol.*, **2**, 125 (2012).
6. J. Sun, C. Sun, X. Lin, X. Cheng, and H. Liu, "Effect of chromium on corrosion behavior of P110 steels in CO₂-H₂S environment with high pressure and high temperature," *Materials*, **9**, 200 (2016).
7. B. Laurent, R. Harrington, and B. Bennett, *Development of test methods and factors for evaluation of oilfield corrosion inhibitors at high temperature, no. 9780*, NACE International, New Orleans, LA (2017).
8. H. Mansoori, R. Mirzaee, F. Esmailzadeh, A. Vojood, and A. Dowran, "Pitting corrosion failure analysis of a wet gas pipeline," *Eng. Fail. Anal.*, **82**, 16 (2017).
9. H. Ma, X. Cheng, G. Li, S. Chen, Z. Quan, S. Zhao, and L. Niu, "The influence of hydrogen sulfide on corrosion of iron under different conditions," *Corros. Sci.*, **42**, 1669 (2000).
10. W. Sun, S. Nescic, and S. Papavinasam, *Kinetics of iron sulfide and mixed iron sulfide/carbonate scale precipitation in CO₂/H₂S corrosion, no. 06644*, NACE International, San Diego, CA (2006).
11. J. Tang, Y. Shao, J. Guo, T. Zhang, G. Meng, and F. Wang, "The effect of H₂S concentration on the corrosion behavior of carbon steel at 90°C," *Corros. Sci.*, **52**, 2050 (2010).
12. Y. Zheng, B. Brown, and S. Nescic, "Electrochemical study and modeling of H₂S corrosion of mild steel," *Corrosion*, **70**, 351 (2013).
13. J. Ning, Y. Zheng, B. Brown, D. Young, and S. Nescic, "A thermodynamic model for the prediction of mild steel corrosion products in an aqueous hydrogen sulfide environment," *Corrosion*, **71**, 945 (2015).
14. S. Gao, P. Jin, B. Brown, D. Young, S. Nescic, and M. Singer, "Corrosion behavior of mild steel in sour environments at elevated temperatures," *Corrosion*, **73**, 915 (2017).
15. S. Gao, P. Jin, B. Brown, D. Young, S. Nescic, and M. Singer, "Effect of high temperature on the aqueous H₂S corrosion of mild steel," *Corrosion*, **73**, 1188 (2017).
16. S. Gao, B. Brown, D. Young, and M. Singer, "Formation of iron oxide and iron sulfide at high temperature and their effects on corrosion," *Corros. Sci.*, accepted, in press.
17. M. Liu, J. Wang, W. Ke, and E. Han, "Corrosion Behavior of X52 Anti-H₂S Pipeline Steel Exposed to High H₂S Concentration Solutions at 90°C," *J. Mater. Sci. Technol.*, **30**, 504 (2014).
18. R. Thodla, F. Gui, K. Evans, C. Joia, and I. P. Baptista, *Corrosion fatigue performance of super 13 CR, duplex 2205 and 2507 for riser applications, no. 10312*, NACE International, San Antonio, TX (2010).
19. T. Tanupabrunsun, B. Brown, and S. Nescic, *Effect of pH on CO₂ corrosion of mild steel at elevated temperatures, no. 2348*, NACE International, Orlando, FL (2013).
20. R. Prakash, R. J. Choudhary, L. S. S. Chandra, N. Lakshmi, and D. M. Phase, "Electrical and magnetic transport properties of Fe₃O₄ thin films on GaAs (100) substrate," *J. Phys. Condens. Matter.*, **19**, 1 (2007).
21. A. R. Lennie, K. E. R. England, and D. Vaughan, "Transformation of Synthetic Mackinawite to Hexagonal Pyrrhotite: a Kinetic Study," *Am. Mineral.*, **80**, 960 (1995).
22. S. N. Esmacely, G. Bota, B. Brown, and S. Nescic, "Influence of Pyrrhotite on the Corrosion of Mild Steel," *Corrosion*, **74**, 37 (2018).
23. H. Vedage, T. A. Ramanarayanan, J. D. Mumford, and S. N. Smith, "Electrochemical Growth of Iron Sulfide Films in H₂S-Saturated Chloride Media," *Corrosion*, **49**, 114 (1993).
24. L. Zhang, J. Yang, J. Sun, and M. Lu, *Effect of Pressure on Wet H₂S/CO₂ Corrosion of Pipeline Steel, no. 09565*, NACE International, Atlanta, GA (2009).

25. W. Li, Y. Zhou, and Y. Xue, Corrosion Behavior of 110S Tube Steel in Environments of High H₂S and CO₂ Content, *J. Iron Steel Res. Int.*, **19**, 59 (2012).
26. T. Tanupabrungsun, Thermodynamics and kinetics of carbon dioxide corrosion of mild steel at elevated temperatures, *Ph.D thesis, Dept. of Chem. Eng.*, Ohio University, Athens, OH, 2013.
27. L. G. Benning, R. T. Wilkin, and H. L. Barnes, "Reaction pathways in the Fe-S system below 100°C," *Chem. Geol.*, **167**, 25 (2000).
28. Y. Zheng, J. Ning, B. Brown, and S. Neise, "Advancement in predictive modeling of mild steel corrosion in CO₂- and H₂S-containing environments," *Corrosion*, **72**, 679 (2016).
29. T. A. Ramanarayanan and S. N. Smith, "Corrosion of iron in gaseous environments and in gas-saturated aqueous environments," *Corrosion*, **46**, 66 (1990).
30. P. Sarin, V. L. Snoeyink, D. A. Lytle, and W. M. Kriven, "Iron corrosion scales: model for scale growth, iron release, and colored water formation," *J. Environ. Eng.*, **130**, 364 (2004).
31. T. Borch, A. K. Camper, J. A. Biederman, P. W. Butterfield, R. Gerlach, and J. E. Amonette, "Evaluation of characterization techniques for iron pipe corrosion products and iron oxide thin films," *J. Environ. Eng.*, **134**, 835 (2008).